Fire Performance of Solid Aluminium of Composite Cladding Panels Incorporating Intumescent Coatings

Touha Nazrun[1], Md Kamrul Hassan[1,*], Md Rayhan Hasnat[1], Md Delwar Hossain[1], Swapan Saha[1]

[1] School of Engineering, Design and Built Environment, Western Sydney University, Penrith, NSW 2751, Australia;

Abstract

The use of solid aluminium as the outer layer of aluminium composite panels (ACP) has raised concerns about fire safety in high-rise buildings. Solid aluminium begins to melt at approximately 660°C, which can exacerbate fire hazards by transferring significant heat from the fire exposed to unexposed sides. This research investigates the fire performance of solid aluminium when treated with two different intumescent coatings (Coating-A and B). The study evaluates solid aluminium with/without coatings to determine their effectiveness in mitigating fire risks. Comprehensive analysis for material characterisation and fire test were conducted to assess the microstructure, elemental composition, and thermal degradation and fire behaviour of the coatings. The findings reveal that while solid aluminium presents significant fire risks when exposed to high temperatures, intumescent coatings can substantially improve fire resistance of solid aluminium. Coating-A, when applied to both sides of the aluminium, reduces melting but still allows some flame spread. In contrast, Coating-B provides exceptional fire protection, preventing melting and flame spread when applied to one side. However, the potential hazard of airborne char particles from Coating-B is the key issue. These results underscore the effectiveness of intumescent coatings to enhance fire safety in solid aluminium cladding.

Keywords: Intumescent coatings, Fire safety, Solid aluminium panels, Aluminium composite panels.

*Correspondence: k.hassan@westernsydney.edu.au

1. INTRODUCTION

The use of advanced lightweight materials, such as aluminium composite panels (ACP), polymers, and fibre-reinforced composites, has increased in exterior cladding systems due to

their excellent thermal insulation, weather resistance, and aesthetic finishes. However, these lightweight materials are flammable and pose significant fire risks to human life, the environment and the economy [1-3]. In recent years, several fire incidents occurred involving external cladding systems. For example, Injuries and deaths occurred as a result of fires in the Milan tower block, Italy in 2021 [4], Neo 200 Building, Melbourne, Australia, in 2019 [5], Dwelling Building, Jecheon, South Korea in 2017 [6], Marina Torch Tower, Dubai, UAE, in 2017 [7], Hotel The Address, Dubai, UAE, in 2016 [7], and Nasser Tower, Sharjah, UAE in 2015 [7]. The causes of these fires varied and included combustible ACP, flammable cladding, and insulation [1-3, 8]. Fire protection for external cladding has become a critical global issue [9]. There are two types of fire protection systems: active and passive fire protection. Active fire protection includes detecting, controlling, and extinguishing fires. This system can be used for both automatic fire alarms and fire detectors, as well as manual fire extinguishers and hydrant boxes [10, 11]. On the other hand, passive fire protection involves materials that can withstand high temperatures without losing mechanical strength, such as intumescent coating materials that help prevent and ensure safe evacuation by providing fire resistance [12].

Solid aluminium is a highly sustainable metal due to its recyclability, durability, and energy efficiency, which is widely used in ACP panels. With a long lifespan of 30 to 50 years, its resistance to weather and corrosion ensures low maintenance costs. These qualities make it an excellent choice for a wide range of applications in the building industry, including façades, windows, and cladding [13]. Solid aluminium has a higher strength-to-weight ratio and offers significant weight reduction due to its lightweight properties [13, 14]. However, solid aluminium has a major drawback: it has a relatively low melting point of around 660 °C and begins to lose its strength around 150°C [15]. Recent fire incidents in the UK, Australia, and other countries have revealed that the solid aluminium used as outer layer in the ACP panels significantly contributed to fire hazards in high-rise buildings [16-18]. Many research work

[19, 20] has been published to improve the fire performance of the core materials of ACP panels. Additionally, much research successfully improved the fire performance of core materials of ACP panels [21]. However, a limited research study is conducted to improve the melting issue of the solid aluminium used as outer skin in the ACP panels. Intumescent coatings can be a highly recommended and effective solution for safeguarding aluminium against fire incidents, providing a valuable protective measure.

Intumescent coatings are fire-retardant paints which react under fire exposure and significantly expand many times to their original thickness in a controlled manner by negating the carbonaceous char. The thick layer of insulating carbonaceous char protects the substrate material from fire damage. Additionally, it helps to provide additional time for occupants to escape safely in a fire incident by trapping fire and smoke [22]. The thick char layer has low thermal conductivity and acts as a thermal insulator during the fire, which helps to prevent a significant temperature rise to the fire-exposed and unexposed sides and protects the structure from collapsing [23]. Intumescent coatings are formulated with three major components: ammonium polyphosphate (APP), which acts as the acid source; pentaerythritol (PER), which serves as the carbon source; and melamine (MEL), functions as the blowing agent. This process produces carbonaceous and phosphocarbonaceous residues, leading to the formation of a char layer [24, 25].

Intumescent coatings have a diverse application on steel [26], wood [27, 28], timber [29] and concrete materials [30, 31], yet their application on the outer layer of ACP has not been explored. The melting of the outer layer of ACP is a common issue nowadays. The char of intumescent coating can protect aluminium on the outer surface of ACP panels when exposed to fire. However, selecting the appropriate coating for application is a big challenge due to the diversity of available commercial products. They are different from each other in their chemical composition, application methods, and levels of fire protection. Additionally,

their effectiveness can vary significantly based on the specific conditions of a fire. Therefore, a proper investigation is needed in the field of fire protection by addressing the overlooked issue of solid aluminium melting in ACPs, proposing intumescent coatings as a viable solution for improving the fire resistance of solid aluminium skin used in the composite cladding panels.

To address the above issues, this study focuses on exploring the fire behaviour of solid aluminium coated with two distinct types of intumescent coatings, each with different chemical compositions and fire performance characteristics. This research paper aims to investigate the influence of these coatings on char formation and their ability to provide fire protection to solid aluminium skin used in ACPs under fire conditions of 1000°C and offer insights into their potential application for enhancing fire safety in building cladding systems.

2. EXPERIMENTAL DETAILS

2.1 Test specimens

In this study, solid aluminium panels with and without intumescent coating have been investigated experimentally. A total of 8 test specimens for three different categories of solid aluminium panels with and without applying coating tests were prepared in this study to conduct the fire tests. Each specimen was cut into the dimensions of 200 mm × 200 mm. Two distinct water-borne fire-retardant coatings were purchased from commercial sources to apply the coating on the solid aluminium panels. These two coatings are introduced in this study as Coating-A and Coating-B. These coatings are referred to as non-toxic and non-hazardous fire-retardant coatings by their respective manufacturers. The thickness of the solid aluminium for all specimens was considered 0.5 mm thick because this thickness is widely used as the outer skin of aluminium composite panels (ACP). In the first category, two specimens were prepared without applying the intumescent coating (SP-C-0), see **Table 1**. In the second category, two specimens were prepared to investigate the effect of Coating-A applied on one side of the panel (SP-C-A). In the third category, two specimens were prepared for Coating-B applied on one

side of the panel (SP-C-B). In the fourth category, another two specimens were prepared for Coating-A(SP-C-A-D) to investigate the effect of Coating-A on both sides. The measured thicknesses of applying Coating-A and B are reported in **Table 1**. It is worth noting that the surfaces of the solid aluminium were cleaned and dried properly before applying both coatings. After the completion of the coatings being applied to the aluminium panels, a drying period of four days was ensured for the coatings to dry completely.

Table 1 Test specimen details of solid aluminium panels with and without coating

Sample Category	Sample label	Dimension (width × depth)	Total thickness	Coating type	Coating thickness	No of specimens
Category 1	SP-C-0	200 × 200	0.5	-	-	2
Category 2	SP-C-A	200 × 200	1.5	A	1.0	2
Category 3	SP-C-B	200 × 200	1.5	B	1.0	2
Category 4	SP-C-A-D	200 × 200	2.0	A	1.5 (1+0.5)	2

2.2 Fire testing using Butane Torch

The butane torch test was employed to evaluate the fire performance of Coating-A and B on the aluminium panel. Natural gas was used as a fuel in this test, and the test was performed in an open environment. Three K-type thermocouples were used to monitor the temperatures of the fire, the front surface of the sample (i.e., fire-exposed side), and the back surface of the sample (i.e., fire unexposed side), see **Figure. 1**. The temperature readings of each thermocouple were recorded at every one-second time interval using a data logger connected to a laptop. Once the fire temperature reached around 1000 °C, the fire temperature was kept constant for the remaining testing time. It is worth mentioning that each specimen was placed at an identical distance from the torch, which was 10 cm. Additionally, each coated sample was exposed to the flame for a standardised duration of 10 minutes, similar to previous research [32].

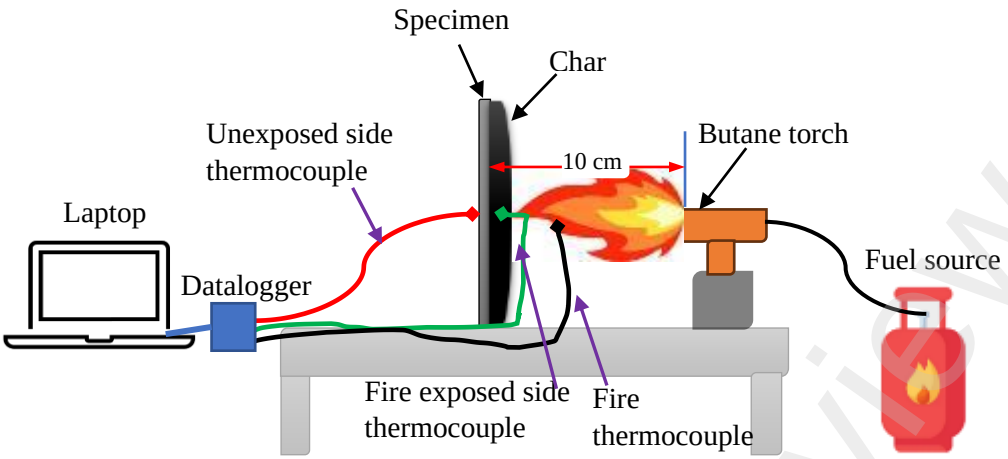

Figure 1: Test setup used for fire testing of solid aluminium with intumescent coating.

2.3 Characterisation of intumescent coating and char

2.3.1 Thermogravimetric analysis

Thermal degradation and mass loss of both coatings were investigated through thermogravimetric Analysis (TGA). The analysis was assessed by using a TGA instrument. The coating samples were heated with temperature from room temperature to 1000°C, at a rate of 10°C per minute under an air atmosphere.

2.3.2 Scanning electron microscopy with EDS

Scanning electron microscopy (SEM)-energy dispersive X-ray spectroscopy (EDS) analysis was conducted to understand micro- and nanoparticle imaging characterisation of both coating materials. SEM (model JEOL 6510LV) with EDS detector analysed the coating samples before and after the fire test. The EDS working distance was 15mm. Using the SEM, 500 µm, 100 µm, 50 µm and 10 µm images were taken of the coating samples.

2.3.3 X-ray diffraction

The mineralogical composition of the coating sample was identified by using X-ray diffraction (XRD) (2019 model). CuKα radiation was used to analyse the coating sample as the X-ray source. The analysis covered a 2θ range of 5° to 90°. The instrument utilised a LynxEye

XE-T detector with a fixed slit size of 0. 20°. The instrument operated at 40kV and 40mA power sources, and the run time was approximately 1 hour and 11 minutes.

2.3.4 Fourier transform infrared spectroscopy

Fourier Transform Infrared Spectroscopy (FTIR) spectra were obtained using a Bruker Vertex 70 FTIR spectrometer, also from Germany. The spectra were collected using a Diamond Attenuated Total Reflection (ATR) accessory with a resolution of 4 cm^{-1}, averaging 32 scans per measurement. The spectral range covered was from 600 cm-1 to 4000 cm^{-1}.

A 6 mm diameter of sample area was used for analysis, and the data were recorded in absorbance units. To ensure accurate measurements, background correction was performed before each new sample set to account for any environmental effects in the laboratory.

3. RESULT & DISCUSSION

3.1 Temperature profile at fire exposed and unexposed sides of solid aluminium panel without coating

The fire behaviour of 0.5mm solid aluminium without coating (SP-C-0 specimen) was investigated using a butane torch, and the temperature-time curves of fire, exposed and unexposed sides of the SP-C-0 specimen, as shown in **Figure 2(a)**. It can be seen that the temperature at the exposed side increases linearly with an increase in the fire temperatures until 872 °C. However, the temperature at the unexposed side does not increase linearly after the temperature of the exposed side is 660°C. This could be due to the melting of aluminium at 660 °C. After melting solid aluminium, the temperature at the unexposed side increases non-linearly until the fire temperature of 967 °C and then increases rapidly when the fire temperature reaches around 970 °C, as shown in **Figure 2(b)**. This could be due to the rapid onset of melting of aluminium and forming a hole on the centre of the specimen **(Figure 3)**. It can be noted that the melting areas of aluminium become like the ash of paper material burning.

166 This behaviour of aluminium is aligned with the previous research reported in the literature
167 [33].

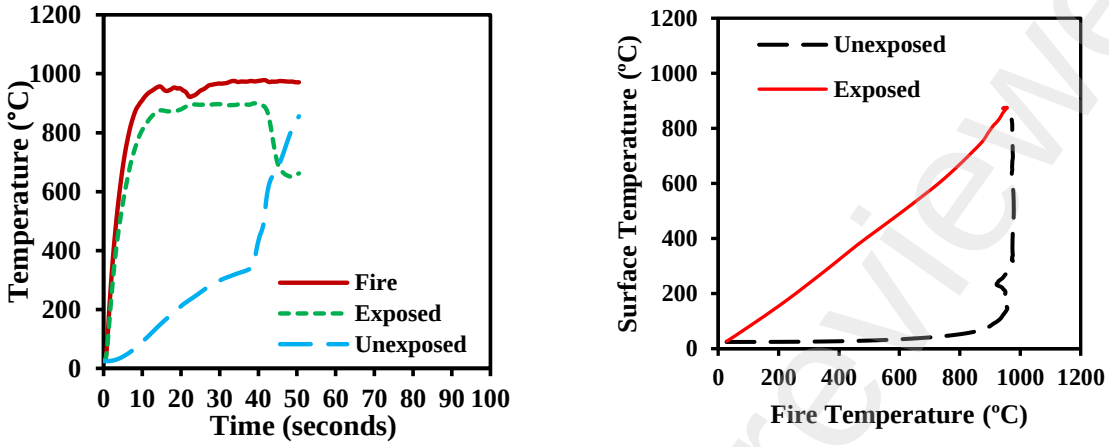

168

169 (a) Time vs temperature curves (b) Fire vs surfaces temperatures

170 **Figure 2:** Fire behaviour of SP-C-0 specimen without coating

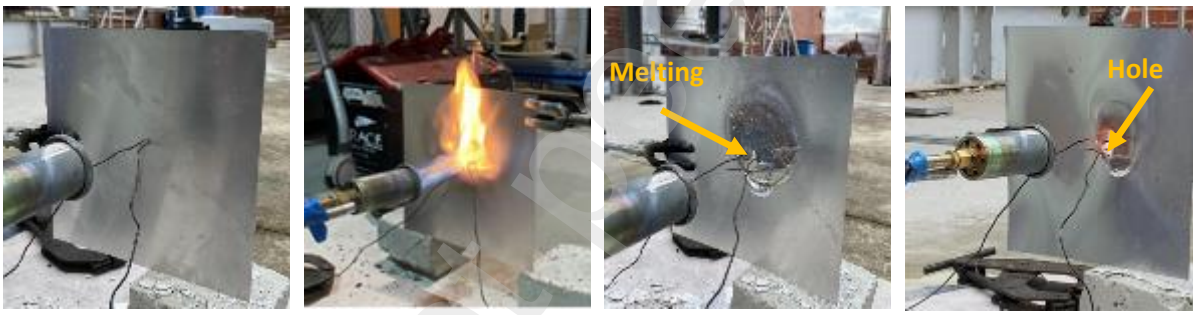

(a) Before testing (b) During testing (c) Specimen melting (d) After testing

171 **Figure 3:** Photos of SP-C-0 specimen without coating during and after fire testing

172

173 **3.2 Effect of Coating-A on the temperature profile at fire exposed and unexposed sides**
174 **of solid aluminium panels**

175 Specimen SP-C-A and SP-C-A-D are coated with Coating-A. Each aluminium panel
176 has a different thickness (see **Table 1**). As reported in the previous section, Specimen SP-C-A
177 has one side coating on the fire-exposed side with a thickness of 1.0 mm, and specimen SP-C-
178 A-D has both sides coating, fire-exposed side of 1.0 mm and unexposed side of 0.5 mm. The
179 test results of the single-side and both sides coating are discussed below.

(a) Coating-A applied on one side (fire exposure side)

Figure 4 shows the temperature profiles of SP-C-A. The measured temperature vs time curves of fire, exposed side and unexposed side of specimen SP-C-A are presented in **Figure 4(a).** In contrast, **Figure 4(b)** demonstrates the exposed and unexposed side's temperatures against the fire temperature. It can be seen from **Figure 4(b)** that the temperature at the fire-exposed side increases linearly with the increase in fire temperatures to 660°C. The temperature at the exposed side is higher than the fire temperature until 800°C **(Figure 4(a))**. This could be due to the ignition of the coating materials. It is worth noting that when fire is applied to the sample SP-C-A, Coating-A ignites first and then burns for a period before giving protection, see **Figure 5(b)**. The main reason for the burning of Coating-A is the presence of hydrocarbon in Coating-A. This proves that after a certain period of fire exposure, the aluminium panel with Coating-A becomes vulnerable due to the flame spreading vertically. After forming the char, the exposed side temperature is lower than the fire temperature **(Figure 4(a))**. However, the char did not protect the aluminium panel effectively from melting due to the thinner char layer, see **Figure 5(c)**. As a result, the unexposed side temperature increases significantly until 1000°C and then increases rapidly, see **Figure 4(b)**. This could be due to the melting of solid aluminium on the back side of the specimen, as seen in **Figure 5(d)**, and the occurrence of hole formation during the experiment. The experiment had to be prematurely terminated due to the occurrence of a hole in the sample. Based on this test, it can be concluded that the protection capabilities of Coating-A applied on one side are very limited in time, and melting is still observed as a key issue.

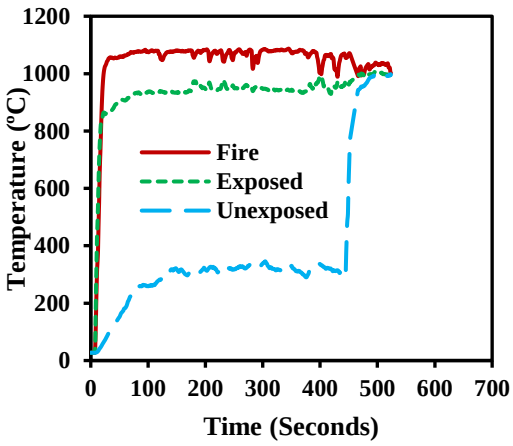

(a) Time vs temperature curve

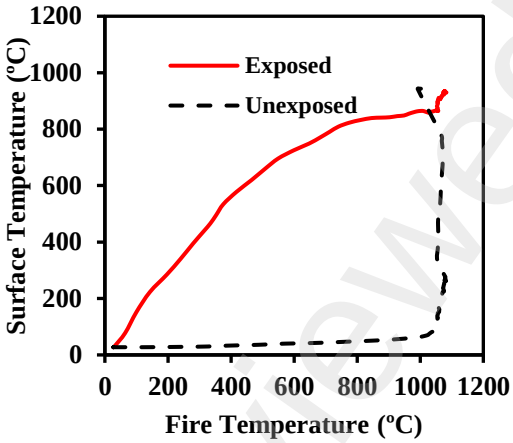

(b) Fire vs surfaces temperature curve

Figure 4: Fire behaviour of SP-C-A specimen with one side Coating-A

(a) Before testing (b) Initial char formation (c) Fully char formed (d) Unexposed side After testing

Figure 5: Photos of tested specimen SP-C-A during and after fire testing

(b) Coating-A applied on both sides (fire exposed and unexposed sides)

The temperature profile of Coating-A applied on both sides of Specimen SP-C-A-D is reported in **Figure 6**. The coating thickness (1 mm) on the exposed side of SP-C-A-D is the same as that of the specimen SP-C-A. As a melting issue on the back side of SP-C-A was observed, 0.5 mm Coating-A was applied to the unexposed side of SP-C-A-D to check the effectiveness of Coating-A. The temperature profile with respect to the time of fire and exposed and unexposed sides of the SP-C-A-D specimen is shown in **Figure 6(a)**. **Figure 6(b)** shows fire temperature vs both surface temperature curves of the specimen SP-C-A-D. It can be observed that the temperature on the exposed side and unexposed side increases linearly until around 909 °C and 620 °C. When specimen SP-C-A-D is exposed to the fire, the coating

initially ignites similarly to the specimen SP-C-A. It burns temporarily on both sides (exposed and unexposed). This ignition and burning causes a rapid temperature increase on the unexposed side **(**as shown in **Figures 6(a-b)**). However, after the burning phase, the coating provides effective protection, leading to a subsequent temperature drop on the unexposed side, as shown in **Figures 6(a-b)**. **Figure 7(b)** indicates that the coating ignites before complete charring, and **Figure 7(c)** shows that no more flame spread was noticed on the coating after complete char formation. The Coating-A applied on both sides of the SP-C-A-D specimen successfully protected the aluminium panel from melting and didn't have any holes on the specimens, as shown in **Figure 7(d)**. However, the maximum temperature observed on the unexposed side of specimen SP-C-A-D A (620 °C) during the fire exposure of 400 seconds was higher compared to the SP-C-A specimen applied only one side Coating-A (325 °C). Based on this test, it can be concluded that the melting issue of solid aluminium can be mitigated by applying Coating-A on both sides, but the flame spread is still a key issue when Coating-A is used.

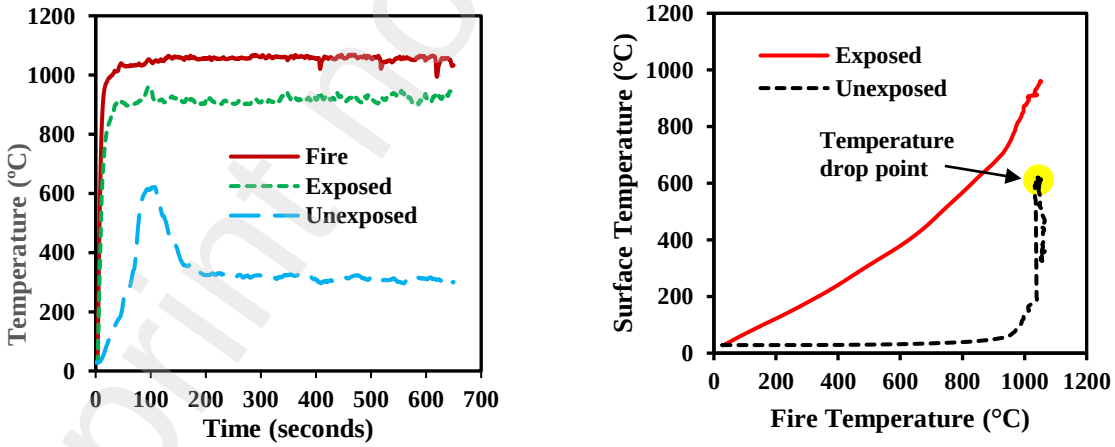

(a) Time vs temperature curves (b) Fire vs surface temperature curves

Figure 6: Fire behaviour of SP-C-A-D specimen with double sides Coating-A

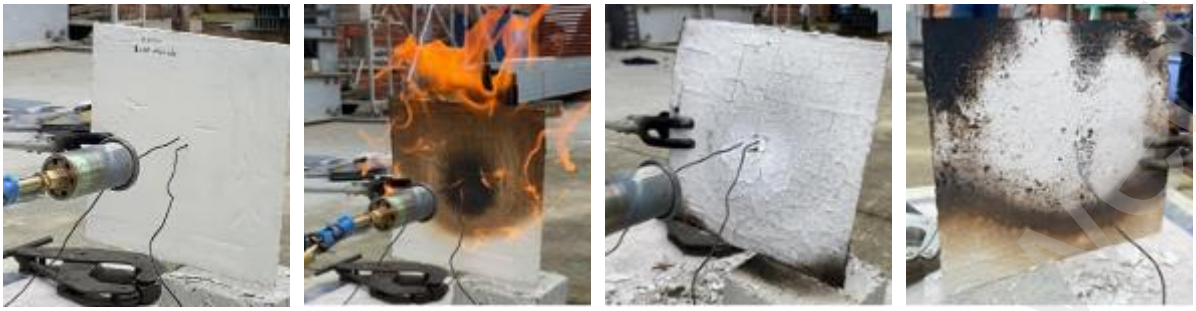

(a) Before testing (b) Initial char formation (c) Fully char formed (d) Unexposed side After testing

Figure 7: Photos of SP-C-A-D specimen during and after fire testing

3.3 Effect of Coating-B on the temperature profile

The effect of Coating-B on the temperature profile of a 0.5mm solid aluminium (SP-C-B specimen) is investigated, and the temperature-time curves of fire, exposed and unexposed sides of the SP-C-B specimen were measured as shown in **Figure 8(a)**. **Figure 8(b)** depicts the fire temperature vs both sides' surface temperature curves of the SP-C-B specimen. It can be seen from **Figure 8(a)** that the temperature at the exposed side initially suppressed the fire temperature until around 520°C due to chemical reactions that occurred during char formation, and the unexposed side of the SP-C-B specimen is observed to be lower compared to the fire temperature. Even the temperature of the exposed side linearly increased until around 627°C, and then the temperature dropped to around 500°C, as shown in **Figure 8(b)**. This temperature drops due to the intumescent Coating-B that undergoes a transformative reaction when exposed to fire, forming a thick, grey-blackish char, as shown in **Figure 9(b)**. In direct interaction with fire, the Coating-B reacts by forming a substantial char layer that offers effective fire protection. Analysis of the results reported in **Figure 8** reveals not only the char formed at the temperature around 630°C **(**as shown in **Figure 9(b))** but also a distinct pattern: the temperature on the exposed side gradually increases until it reaches a peak, after which it stabilises around 490°C. Similarly, the unexposed side experiences a sudden spike followed by a consistent temperature of around 150°C, as shown in **Figure 8(b)**. The reason behind this behaviour is

the char formation process. As the char layer develops **(**as shown in **Figure 9(c))**, it acts as a fire barrier and heat-resistant barrier that mitigates heat transfer, which leads to a temperature drop on the exposed side. On the other hand, the unexposed side efficiently absorbs and disperses heat from the exposed side, which leads to the initial temperature. After the stable char formed, the temperature of the exposed and unexposed sides remained constant. Coating-B shows exceptional fire protection performance. **Figure 9(d)** shows the well-preserved condition of the aluminium after the test, and there is no melting issue when Coating-B is applied to one side of specimen SP-C-B. However, black particles are generated during the burning of chars of Coating-B, which move upward during the fire, which could create a fire hazard, and this hazard could be more significant if there is a strong wind.

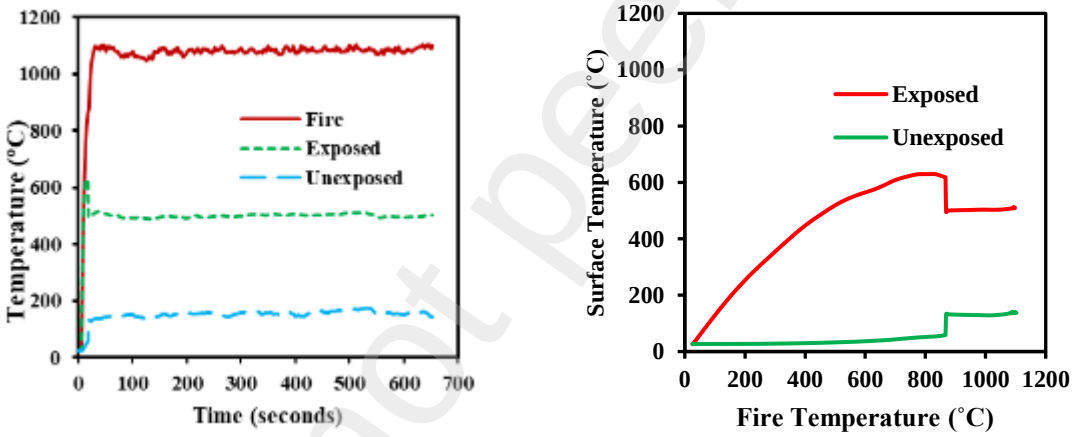

(a) Time vs temperature curve (b) Fire vs surfaces temperature curve

Figure 8: Fire behaviour of SP-C-B specimen with oneside with Coating-B

(a) Before testing (b) Initially char formation (c) Fully char formed (d)Unexposed side after testing

Figure 9: Photos of SP-C-B specimen during and after fire testing

3.4 Flame spread and char formation for Coating-A and Coating-B

The fire spread and char formation with fire exposure time are illustrated in **Figure 10** for Coating-A and in **Figure 11** for Coating-B. It can be seen from these two figures that the fire spread and the char formation of both coatings are not the same. This could be due to the different compositions used to prepare the coating in their formulation. In Coating-A, the fire spread is observed significantly due to the presence of petroleum in Coating-A, which makes it combustible. It can be seen from **Figure 10(a)** that Coating-A ignites within 10 seconds when it is exposed to fire. The flame height increases significantly with time and until the burning of the petroleum fuel **(**as shown in **Figure 10b-e)**, and then the flame height **(Figure 10(f))** is reduced by forming the char after the fire exposure of 70 s.

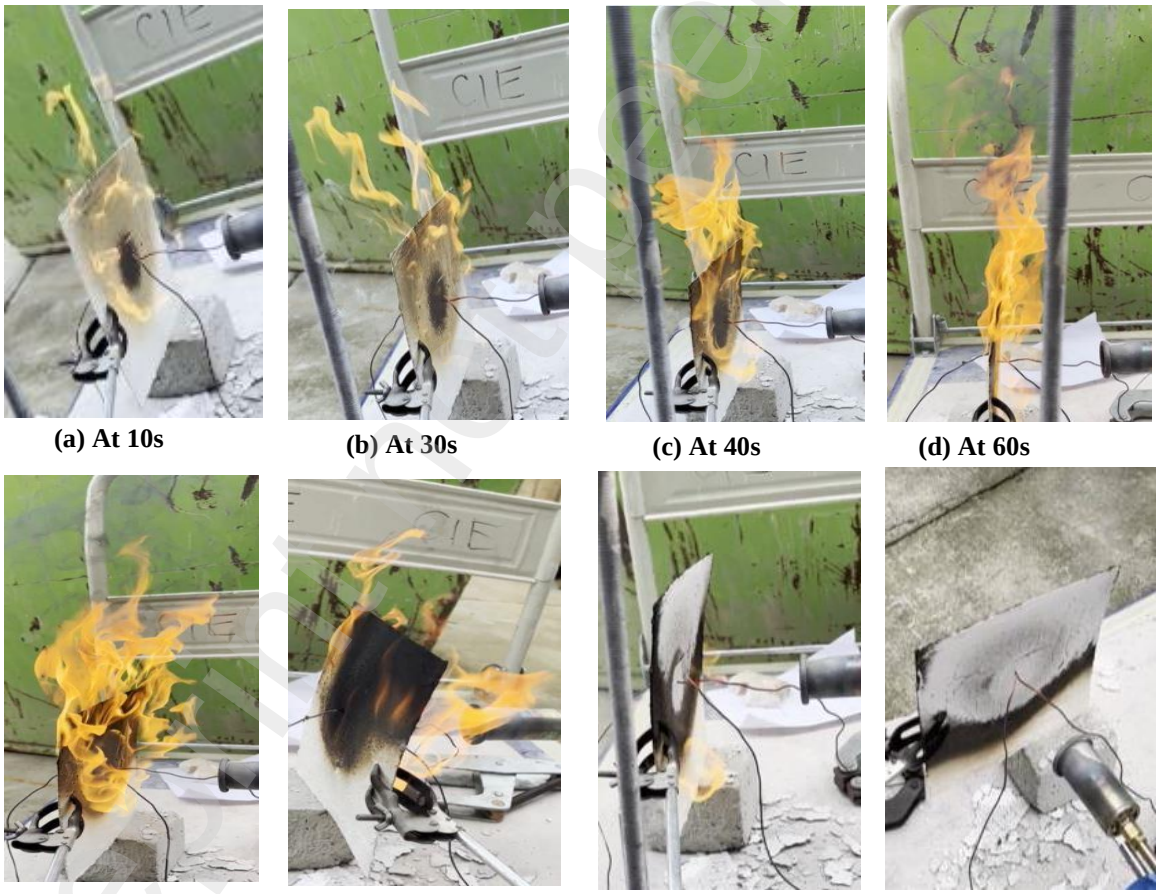

Figure 10: Flame height and char formation stages of Coating-A at different time intervals.

The fire spread slows due to the depletion of the fuel source. Significant smoke is observed at the peak flame stage **(Figure 10(d))**. This could be due to the presence of calcium carbonate, which contributes to smoke production by releasing carbon dioxide when exposed to fire. After 100 s of fire exposure, the char layer is observed significantly **(Figure 10(g)),** and once a complete char layer forms **(Figure 10(h)**), the fire ceases to spread and gives the fire protection to the substrate. The char thickness for Coating-A was nearly similar to the coating thickness.

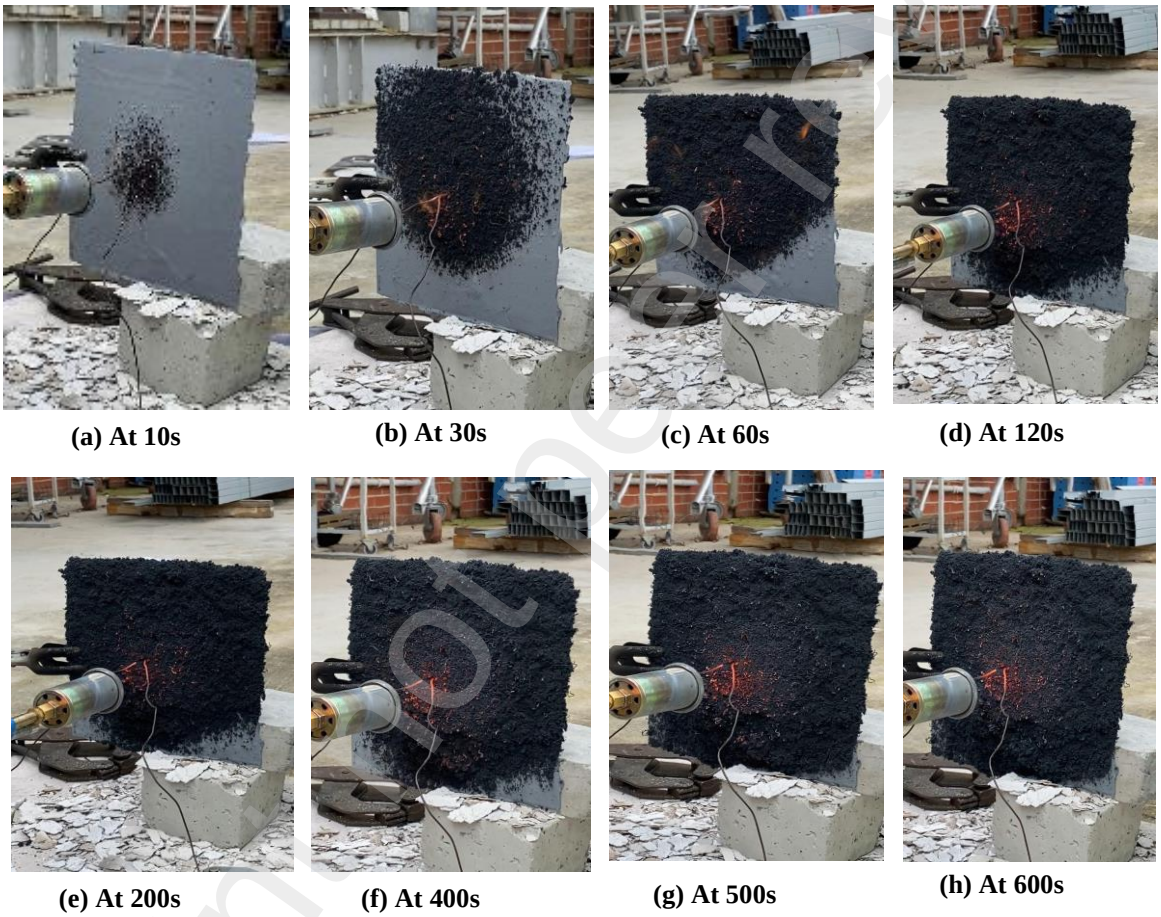

Figure 11: Photos of fire testing of Coating-B at different time intervals.

There is no flame spread in Coating-B when exposed to the fire. The char formation of Coating-B is not similar to Coating-A. **Figure 11** shows the various stages of char formation of Coating-B**.** When the Coating-B is exposed to the fire, the char formation starts initially, as shown in **Figure 11(a-b**). At the early stage of fire exposure (10 s), the key materials undergo chemical reactions and form a limited char layer, as shown in **Figure 11(a)**. Over time of fire

exposure, the char formation is observed significantly, and the char layer fully develops, effectively protecting the underlying substrate from further damage, as shown in **Figure 11(c-h)**. During the char formation, the expandable graphite used in Coating-B expands, traps gases formed by chemical reactions, and forms a protective char layer. The maximum char thickness for Coating-B was 21 mm.

3.5 Microstructure analysis for Coating-A and Coating-B

The microstructure of Coating-A and B before the fire testing was analysed by scanning electron microscopy-SEM (model JEOL 6510LV) with EDS detector, as shown in **Figure 12**. The microstructure image of Coating-A at magnifications of 100 µm, 50 µm, and 10 µm is illustrated in **Figures 12(a-c)**. Similarly, pictures of Coating-B at the same magnifications are shown in **Figures 12(d-f)**. Comparing Coating-A to Coating-B, Coating-A shows a more consistent and even structure. It is clear that Coating-B has much larger particles **Figure 12(f)** than Coating-A **Figure 12(c)**, which is caused by the increased filler concentration in Coating-B. Coating-B's particle size is greater because of the increased filler content. Coating-A offers a smoother surface and a superior external finish on an aluminium sheet.

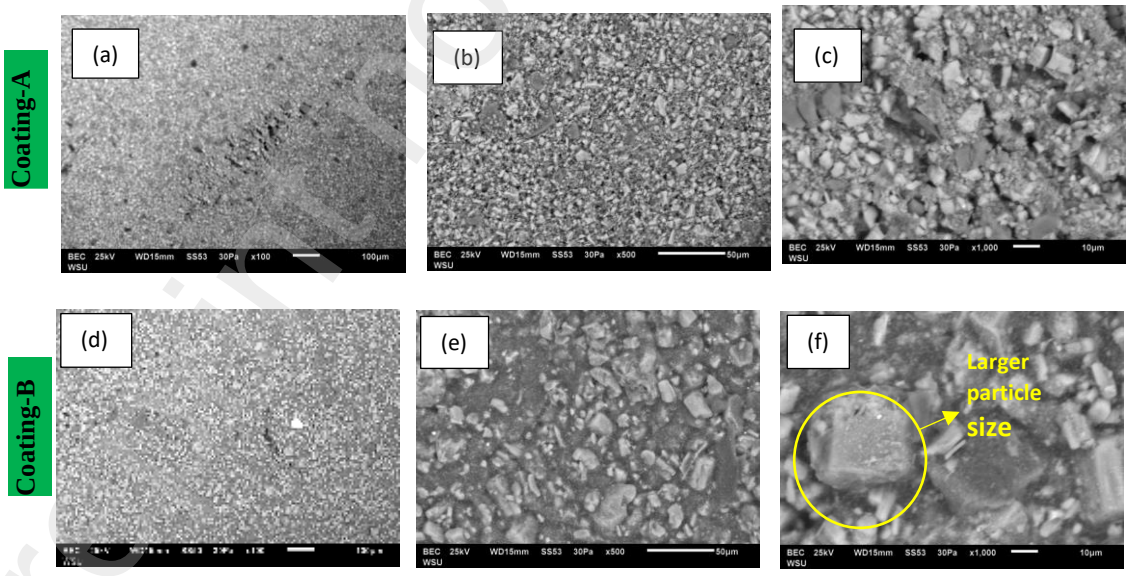

Figure 12: SEM analysis of Coating-A & Coating-B. a, b and c are the 100, 50 and 10 µm images of Coating-A and d, e and f are the 100 µm, 50 µm and 10 µm images of Coating-B.

Figure 13 shows the EDS spectrum results of Coating-A and Coating-B. The EDS spectrum indicates that the sample of Coating-A primarily consists of calcium (Ca) with significant peaks. Additionally, other peaks are observed, including carbon (C), oxygen (O), magnesium (Mg), Aluminium (Al), and titanium (Ti). The high calcium peak proves that Coating-A is rich with calcium compounds. The Ca escape peak is an analysis artifact. For Coating-B, the EDS spectrum (**Figure 13**) shows that Coating-B has a significant amount of Aluminium (Al) and phosphorus (P). Furthermore, C, O, Si, and Ti elements are also found in the Coating-B. The EDS spectrum of Coating-B is noisier than Coating-A, which proves that Coating-B has more compounds in it.

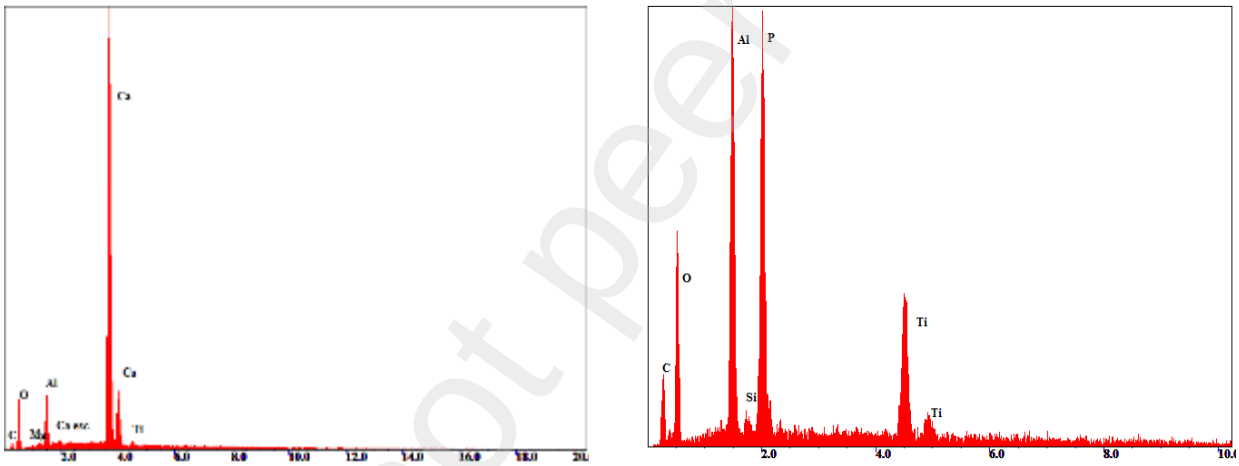

(a) Coating-A **(b) Coating-B**

Figure 13: EDS analysis of Coating-A and Coating-B.

After fire testing for both coatings, the morphology of the internal char structure of Coatings A and B was investigated under SEM with an EDS detector. The microstructures of chars of Coating-A are shown in **Figures 14(a-c)** at magnifications of 100 µm (250×), 50 µm (450×), and 10 µm (1400×). Similarly, the chars of Coating-B at the same magnifications are shown in **Figures 14(d-f)**. It can be seen that the char of Coating-A exhibits a powdery and solid char morphology. Additionally, it shows a cementitious structure with a higher prevalence of cracks compared to the char of Coating-B. In contrast, the char of the Coating-B exhibits a

foam-like and fluffy morphology with a loose structure. This indicates that the gases released during combustion were not confined within the polymer matrix. Additionally, Coating-B has a porous char structure and is well distributed, which helps to transfer the heat from the fire-exposed side to the unexposed side.

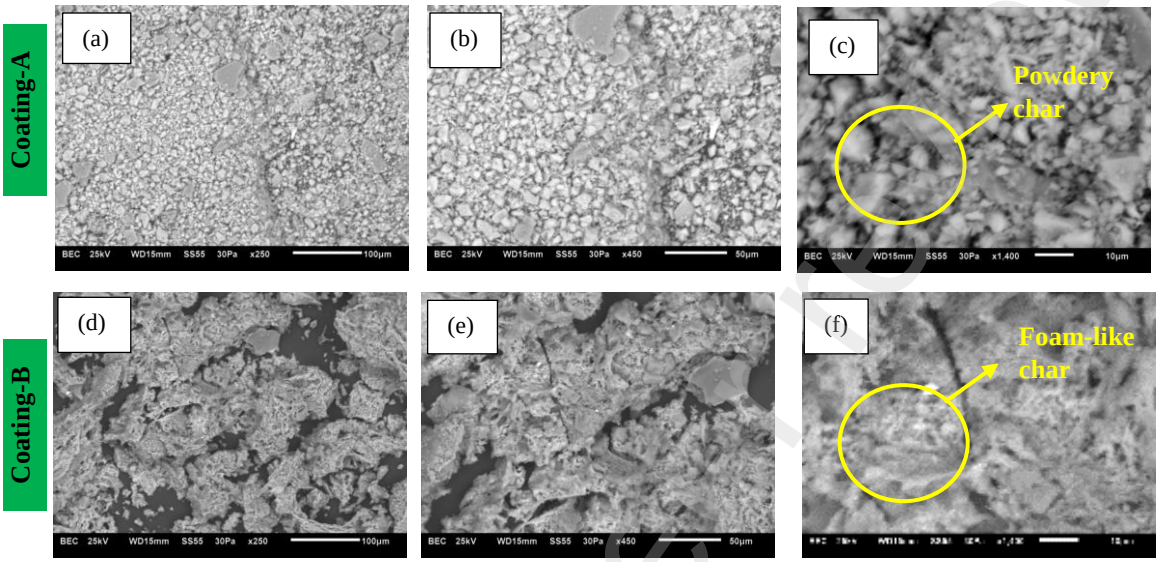

Figure 14: SEM analysis of the char of Coating-A and Coating-B. a, b and c are the 100 µm, 50 µm and 10 µm images of Coating-A and d, e and f are the 100 µm, 50 µm and 10 µm images of Coating-B.

Figure 15 shows the EDS spectrum of char of Coatings-A and Coating-B. The EDS spectrum indicates that the char sample of Coating-A primarily consists of Ca, with significant peaks. Further peaks such as C, O, Mg, Al, Na, and Ti can also be seen in the char of Coating-A. The high calcium peak proves that the char of Coating-A is also rich with calcium compounds. The compositions of Coating-A and its char are similar (**Figure 13(a) and Figure 15(a))**. For Coating-B, the EDS spectrum **(Figure 15(b))** shows that the char of Coating-B has a significant amount of Aluminium (Al). However, the phosphorus (P) has a significant peak in the coating form than the char form **(Figure 13(b) and Figure 15(b))**. Furthermore, C, O, Si, and Ti elements are also found in the char of Coating-B.

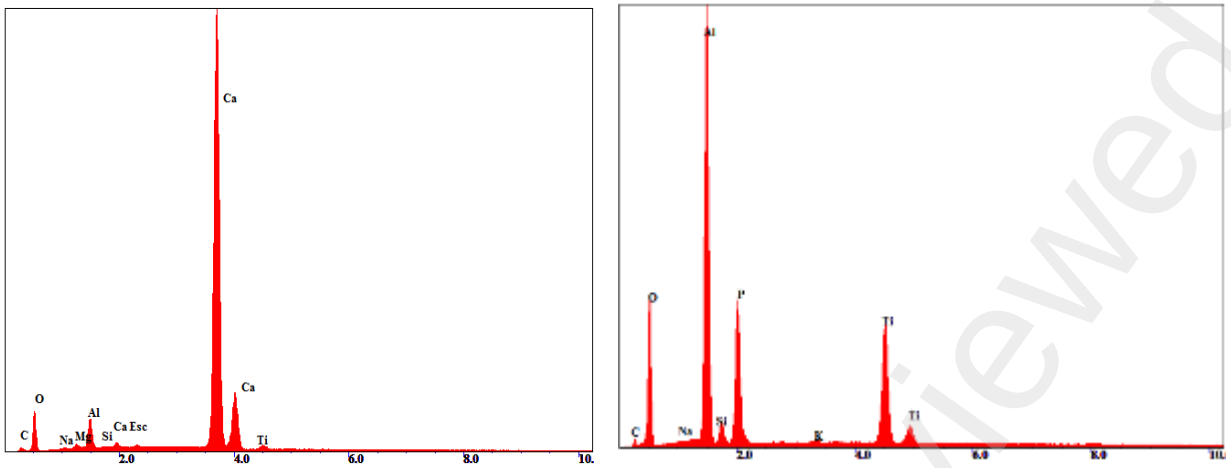

(a) Char of Coating-A **(b) Char of Coating-B**

Figure 15: EDS analysis of char of Coating-A and Coating-B.

3.6 Elementary analysis and chemical reaction studies

An elementary analysis using XRD for Coating-A and Coating-B samples before and after fire testing is conducted to understand the chemical reaction in the coating. **Figure 16(a-c)** shows the XRD patterns of the solid aluminium panel, Coating-A and Coating-B samples. Similarly, **Figure 16(d-c)** shows the XRD patterns of the char of Coatings-A and Coating-B. The XRD patterns reveal key insights into sample composition and properties. **Figure 16(a)** shows that the characteristic peaks indicate the crystalline structure of aluminium (powder diffraction file (PDF) 04-024-6814), indicating that the solid aluminium panel used in this experiment was made of pure aluminium. In **Figure 16(b)**, it is observed that Coating-A have calcite ($CaCO_3$) (PDF 01-086-4274) and gibbsite ($Al(OH)_3$) (PDF 00-007-0324) as the main ingredients. These materials have excellent thermal stability and mechanical strength. Under heating conditions, gibbsite decomposes into alumina (Al_2O_3) and water (H_2O), where water helps to cool down the surface temperature of the coating, and alumina has high heat resistance properties. Additionally, calcite ($CaCO_3$) breaks down into calcium oxide (CaO) and carbon dioxide (CO_2) when exposed to fire or heat [34], enhancing the coating's thermal resistance.

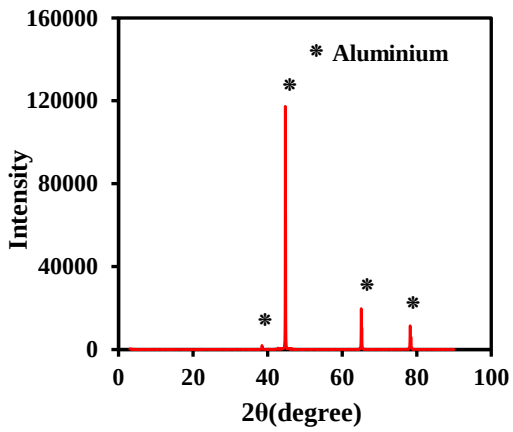

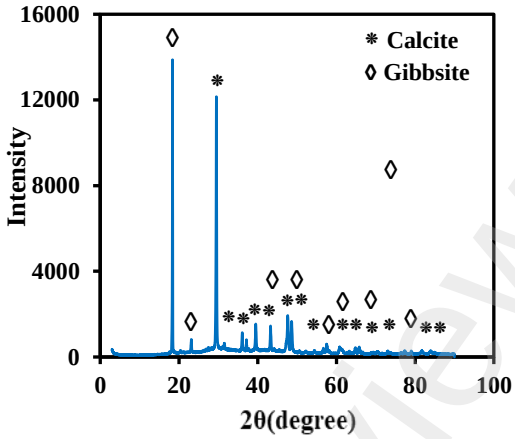

356

357 **(a)** XRD analysis of Aluminium sheet **(b)** XRD analysis of Coating-A

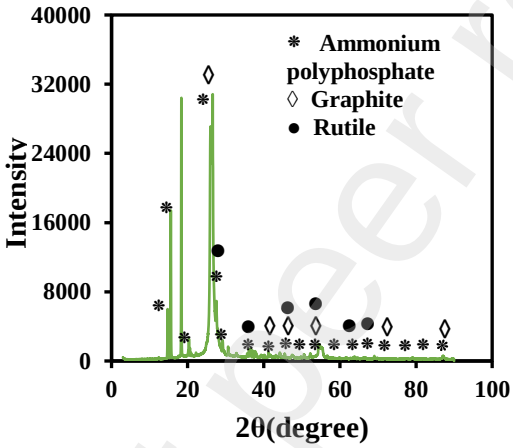

358 **(c)** XRD analysis of Coating-B.

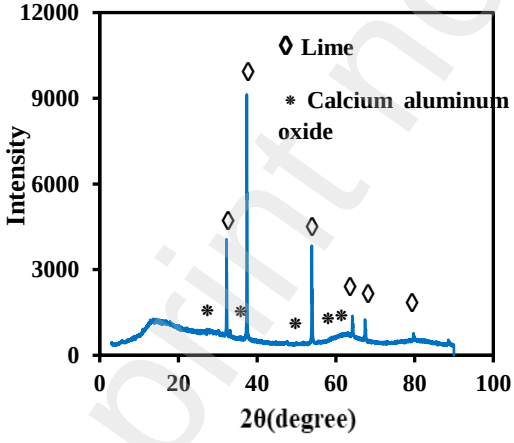

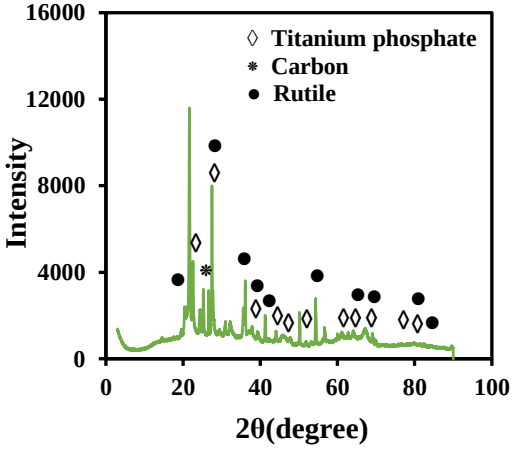

359 (d) XRD analysis of Char of Coating-A (e) XRD analysis of Char of Coating-B

360 **Figure 16:** XRD analysis of solid aluminium sheet, Coating-A and B before fire test and char

361 of Coating-A and Coating-B after fire test.

In the **Figure 16(d),** it is observed that the char of Coating A has lime (CaO) (PDF 01-082-1690), and calcium aluminium oxide ($CaAl_2O_4$) (PDF 00-062-0852). Calcium oxide and aluminium oxide react at high temperatures and produce calcium aluminium oxide. Calcium aluminium oxide is a widely used cement that is used in high-performance applications requiring resistance to chemical attack, high early strength, refractory properties, and abrasion resistance [35].

$$Al(OH)_3 \xrightarrow{Heat} Al_2O_3 + H_2O$$

$$CaCO_3 \xrightarrow{Heat} CaO + CO_2$$

Figure 16(c) shows that Coating-B sample contains ammonium polyphosphate ($(NH_4)PO_3$) (PDF 00-069-0862), graphite (C) (PDF 00-056-0159), and rutile (TiO_2) (PDF 01-078-4190). These compounds react together and form chars that give fire protection to the aluminium sheet.

$$2TiO_2 + (NH_4)_4P_4O_{12} \rightarrow 2TiP_2O_7 + 4NH_3 + 2H_2O$$

Additionally, the interaction between ammonium polyphosphate and titanium dioxide in the fire results in the formation of titanium pyrophosphate (TiP_2O_7), which enhances fire protection capabilities by increasing thermal stability and radiative heat transfer [36]. **Figure 16(e)** proves that the char of Coating-B has titanium pyrophosphate (TiP_2O_7) (PDF 00-052-1470). Additionally, it is also observed that the char of Coating-B has Carbon (C) (PDF 01-086-7889) and rutile (TiO2) (PDF 01-089-8302). This increases residue at higher temperatures, increasing the fire performance.

3.7 FTIR analysis

Figure 17 shows the FTIR spectrum of the internal coating sample of A and B. The two samples have different peaks. For Coating-A, the band at 713 cm^{-1} due to stretching

vibration, 875 cm^{-1} due to bending vibration and 1429 cm^{-1} due to bending vibration are for C-O bond. C-O bond here for calcium carbonate [37-39]. Additionally, the band at 3453 cm^{-1} is for O-H stretching vibrations [40, 41]. There is a strong peak at 1739 cm^{-1}, due to C=O stretching vibration of carbonyl group [42]. This proves that Coating-A contains a carbonyl group (C=O). The band is 2960 cm^{-1} due to C-H stretching vibrations [43, 44]. In the case of Coating-B, the region 1400-800 cm^{-1} showed the presence of phosphate (P-O-P) and 1020 cm^{-1}, 1163 cm^{-1}, and 1250 cm^{-1} confirmed the existence of phosphate PO_4^- due to the presence of APP in the coating formulation [45]. There is a strong peak at 1732 cm^{-1} due to the carbonyl group (C=O) [36]. The peak at 1454 cm^{-1} and 2958 cm^{-1} in Coating-B represents the stretching vibration of CH_2 or CH_3 distortion in vibration due to polyaromatic compounds [46]. Additionally, one bending peak at 3443 cm^{-1} represents the stretching vibrations of $–NH_2$ bonds [47, 48]. The peak at 558 cm^{-1} represents C–C=O in-plane vibration mode [49].

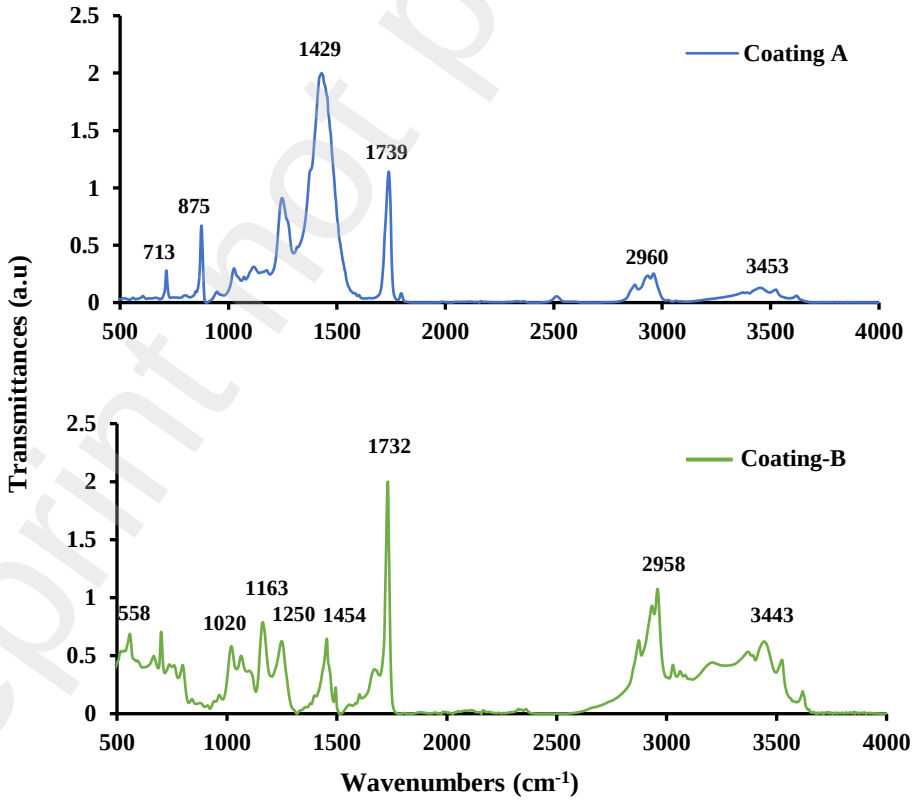

Figure 17: FTIR analysis of Coating-A and Coating-B

3.8 Thermal degradation analysis

The thermal degradation of Coating-A and Coating-B and the amount of char residue at high temperatures were examined by TGA to understand the fire behaviour of coating applied on solid aluminium. **Figure 18 (a-b)** shows the TGA and DTG curves of Coating-A and B. The DTG analysis shows that Coating-A has three major degradation steps. At around 230-360 ºC temperature, a noticeable drop in mass was 18.36%. In the second stage, around 360-450 ºC temperature, an additional 8.45% mass loss occurred. Thermal decomposition or volatilisation of coating components is the reason behind it. The residual mass remains relatively stable around 450-680 ºC, and mass loss was only 2.39%; no significant decomposition has been noticed during this temperature range. A significant mass drop of 25.74% occurred around 680-816 ºC, indicating another decomposition or volatilisation of coating components. Beyond 820 ºC temperature, the curve stabilises, proving the remaining materials are thermally stable up to 1048.2 ºC. At 1048.2 ºC temperature, the residual mass of Coating-A is 44.11% of its original mass. On the other hand, Coating-B has three degradation steps. In the first stage, at the temperature range of 200-380 ºC, 32.15% of weight loss occurred due to the thermal decomposition of coating materials. During the second stage, 380-850 ºC, a more gradual mass loss occurred, proving the continuous decomposition of coating materials and around 20.54% mass loss. A rapid decomposition occurred from 850-950 ºC, and 16% of mass loss occurred. Beyond 850 ºC temperature, the mass continues to decrease gradually and at the 1048.1°C, 28.19% of its original mass remains **(Figure 18(a))**. It can be seen from **Figure 18** that the mass loss of Coating-B is higher than that of Coating-A, and the residual mass of Coating-B is less than that of Coating-A. The reason behind this is that the char volume of Coating-B is much higher than that of Coating-A. For this reason, the fire protection of Coating-B is better than Coating-A, which is also observed during the fire tests discussed in section 3.1 to 3.4.

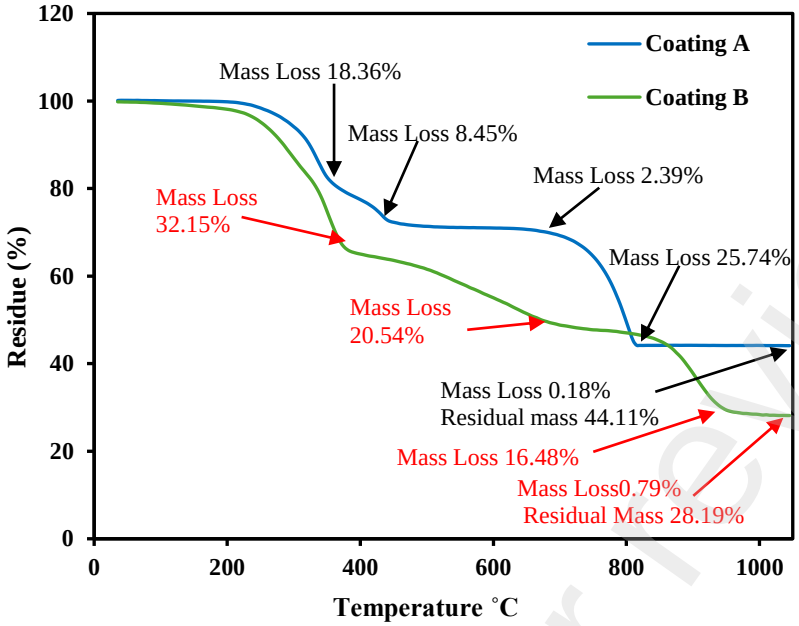

(a) TGA curves of Coating-A and Coating-B

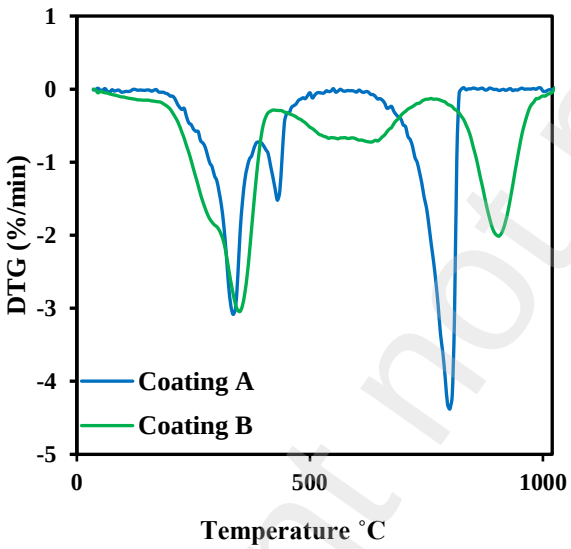

(b) DTG curves of Coating-A and Coating-B

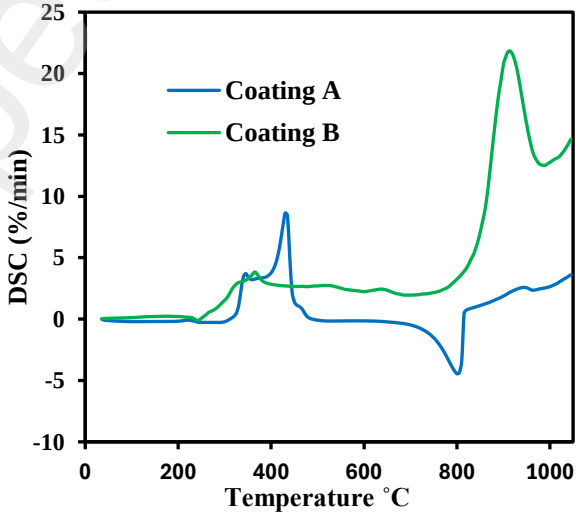

(c) DSC curves of Coating-A and Coating-B

Figure 18: Thermogravimetric Analysis (TGA) of Coating-A and Coating-B

It can be seen from **Figure 18(c)** that the DSC curve for Coating-A shows a broad exothermic peak around 300°C to 500°C, followed by a smaller endothermic peak around 750°C to 830°C. Decomposition of the Coating-A is the possible reason behind the exothermic peak at 300°C to 500°C. This reaction is exothermic. Aluminium hydroxide is an endothermic reaction and can lose water molecules (dehydrate) around 200-300°C. However, the temperature range in

the curve suggests this might be a minor contribution to the overall peak. Calcium carbonate is another component of Coating-A that decomposes around 898℃ and is an endothermic reaction that absorbs heat. **Figure 18(c)** shows that the second peak is around 750°C to 830°C, possibly due to the decomposition of calcium carbonate. Coating-B has a more complicated formulation and more fillers. **Figure 18(c)** shows that Coating-B has two exothermic peaks around 250°C to 400 ℃ and 800°C to 1000°C. The reason behind the exothermic reactions is the decomposition of coating material and the formation of char. Coating-B doesn't absorb heat and produces heat through an exothermic reaction.

4. CONCLUSION

This research study investigates the effectiveness of coating on the outer skin of aluminium composite panels (ACP). In this study, the outer skin, i.e., 0.5mm solid aluminium with and without coating, is tested using a butane torch as the fire source. This study uses two types of coatings (Coating-A and B). Both coatings are non-toxic and water-based intumescent coatings. Based on the scope of this research study, the following conclusions can be drawn:

- Pure solid aluminium used as the outer layer in ACP can create a fire hazard when exposed to high temperatures (>660°C). When the fire temperature on the exposed side of solid aluminium exceeds more than 660°C, it starts to melt and form a hole on the centre of the specimen.
- Intumescent coating could effectively mitigate the melting issue of solid aluminium used as the outer layer in ACP. However, a careful selection of intumescent coating is very important as the fire behaviour of all coating is not the same.
- The melting issue of solid aluminium can be mitigated by applying Coating-A on both sides instead of a single side, but the flame spread is still a key issue when Coating-A is used.

- Coating-B shows exceptional fire protection performance compared to Coating-A. No melting and flame spread issues are observed for Coating-B, although it is applied on one side of specimen SP-C-B. Coating-B exhibits excellent adhesive characteristics on the solid aluminium, maintaining its char integrity even after the fire was extinguished. However, black char particles generated during the burning of chars of Coating-B could create a fire hazard. They can become airborne and pose a hazard to the eyes and respiratory system. Further research can be conducted to mitigate this black char particles generated during the burning of chars of intumescent coating.

ACKNOWLEDGEMENT

The first author gratefully acknowledges the Research Assistantship and material supports provided by Western Sydney University during MPhil study. The authors would also like to express their sincere gratitude to the Advanced Materials Characterisation Facility (AMCF) and the Structural Testing Laboratory at Western Sydney University for providing essential resources and support in conducting the material characterization and fire testing.

Reference

1. Hossain, M.D., et al., *Flame behaviour, fire hazard and fire testing approach for lightweight composite claddings–a review.* Journal of structural fire engineering, 2021. **12**(3): p. 257-292.
2. Hossain, M.D., et al., *Testing of aluminium composite panels in a cone calorimeter: A new specimen preparation method.* Polymer Testing, 2022. **106**: p. 107454.
3. Hassan, M.K., et al., *Numerical investigations on the influencing factors of rapid fire spread of flammable cladding in a high-rise building.* Fire, 2022. **5**(5): p. 149.
4. Mazzucchelli, E., P. Rigone, and B. De la Fuente Ceja, *Fire Safety Facade Design: The case study of an office tower in Milan,* in *Face Time 2020: Better Buildings through Better Skins*. 2020, Tectonic Press. p. 209-223.
5. Yuen, A.C.Y., et al., *Evaluating the fire risk associated with cladding panels: An overview of fire incidents, policies, and future perspective in fire standards.* Fire and materials, 2021. **45**(5): p. 663-689.
6. Wi, S., et al., *Assessment of recycled ceramic-based inorganic insulation for improving energy efficiency and flame retardancy of buildings.* Environment international, 2019. **130**: p. 104900.
7. Guillaume, E., et al., *Study of fire behaviour of facade mock-ups equipped with aluminium composite material-based claddings, using intermediate-scale test method.* Fire and Materials, 2018. **42**(5): p. 561-577.
8. Hossain, M.D., et al., *Fire behaviour of insulation panels commonly used in high-rise buildings.* Fire, 2022. **5**(3): p. 81.
9. Chen, T.B.Y., et al., *Fire risk assessment of combustible exterior cladding using a collective numerical database.* Fire, 2019. **2**(1): p. 11.
10. Mróz, K., I. Hager, and K. Korniejenko, *Material solutions for passive fire protection of buildings and structures and their performances testing.* Procedia Engineering, 2016. **151**: p. 284-291.
11. Suryoputro, M.R., et al. *Active and passive fire protection system in academic building KH. Mas Mansur, Islamic University of Indonesia*. in *MATEC Web of Conferences*. 2018. EDP Sciences.
12. Landucci, G., et al., *Design and testing of innovative materials for passive fire protection.* Fire Safety Journal, 2009. **44**(8): p. 1103-1109.

13. Efthymiou, E., Ö.N. Cöcen, and S.R. Ermolli, *Sustainable aluminium systems.* Sustainability, 2010. **2**(9): p. 3100-3109.
14. Miller, W., et al., *Recent development in aluminium alloys for the automotive industry.* Materials Science and Engineering: A, 2000. **280**(1): p. 37-49.
15. Leitner, M., et al., *Thermophysical properties of liquid aluminum.* Metallurgical and Materials Transactions A, 2017. **48**: p. 3036-3045.
16. Khan, A.A., et al., *Facade fire hazards of bench-scale aluminum composite panel with flame-retardant core.* Fire Technology, 2021: p. 1-24.
17. Maguire, J.F. and L.V. Woodcock, *Thermodynamics of tower-block infernos: effects of water on aluminum fires.* Entropy, 2019. **22**(1): p. 14.
18. Almarzooqi, A., A. Alzubaidi, and S. Alkatheeri. *Fire hazards by aluminum composite cladding in high-rise buildings*. in *Proceedings of the 5th European International Conference on Industrial Engineering and Operations Management, Rome, Italy*. 2022.
19. Gandhi, P., et al., *Performance of glass-ACP façade system in a full-scale real fire test in a G+ 2 structure.* Procedia engineering, 2017. **210**: p. 512-519.
20. Li, K., et al., *Improving the fire performance of structural insulated panel core materials with intumescent flame-retardant epoxy resin adhesive.* Fire Technology, 2023. **59**(1): p. 29-51.
21. *ALPOLIC™ NC / ALPOLIC™ A1, Non-Combustible Claddingprepared by ExcelPlas*. 2021 [cited 2024 19/09/2024]; Available from: https://www.claddingsystems.com.au/20/wp-content/uploads/2022/03/ALPOLIC-NC-White-Paper-Sept-2021.pdf.
22. Kwang Yin, J.J., et al., *Preparation of intumescent fire protective coating for fire rated timber door.* Coatings, 2019. **9**(11): p. 738.
23. de Silva, D., A. Bilotta, and E. Nigro, *Experimental investigation on steel elements protected with intumescent coating.* Construction and Building Materials, 2019. **205**: p. 232-244.
24. Lim, K.-S., et al., *A review of application of ammonium polyphosphate as intumescent flame retardant in thermoplastic composites.* Composites Part B: Engineering, 2016. **84**: p. 155-174.
25. Baena, J.C., et al., *Fire behaviour of waterborne intumescent coatings on timber substrate for bushfire exposure.* Fire Safety Journal, 2023. **140**: p. 103836.
26. Beh, J.H., et al., *Fire protection performance and thermal behavior of thin film intumescent coating.* Coatings, 2019. **9**(8): p. 483.

27. Hussain, A., et al., *Fire performance of intumescent waterborne coatings with encapsulated APP for wood constructions.* Coatings, 2021. **11**(11): p. 1272.
28. Canosa, G., P.V. Alfieri, and C.A. Giudice, *Hybrid intumescent coatings for wood protection against fire action.* Industrial & engineering chemistry research, 2011. **50**(21): p. 11897-11905.
29. Lucherini, A., Q.S. Razzaque, and C. Maluk, *Exploring the fire behaviour of thin intumescent coatings used on timber.* Fire Safety Journal, 2019. **109**: p. 102887.
30. Ghiji, M., P. Joseph, and M. Guerrieri, *Some recent developments and testing strategies relating to the passive fire protection of concrete using intumescent coatings: a review.* Journal of Structural Fire Engineering, 2023. **14**(1): p. 61-89.
31. Li, F.-F., *Comprehensive Review of Recent Research Advances on Flame-Retardant Coatings for Building Materials: Chemical Ingredients, Micromorphology, and Processing Techniques.* Molecules, 2023. **28**(4): p. 1842.
32. Nazaré, S., et al., *Factors for consideration in an open-flame test for assessing fire blocking performance of barrier fabrics.* Polymers, 2016. **8**(9): p. 342.
33. Nurdiansyah, H. and F. Ridha, *Aluminum combustion under different condition: a review.* Journal of Energy, Mechanical, Material, and Manufacturing Engineering, 2020. **5**(2): p. 1-8.
34. Khine, E.E., et al., *Synthesis and characterization of calcium oxide nanoparticles for CO2 capture.* Journal of Nanoparticle Research, 2022. **24**(7): p. 139.
35. Ukrainczyk, N. and T. Matusinović, *Thermal properties of hydrating calcium aluminate cement pastes.* Cement and concrete research, 2010. **40**(1): p. 128-136.
36. Puri, R.G. and A. Khanna, *Effect of cenospheres on the char formation and fire protective performance of water-based intumescent coatings on structural steel.* Progress in Organic Coatings, 2016. **92**: p. 8-15.
37. Vagenas, N.V., A. Gatsouli, and C.G. Kontoyannis, *Quantitative analysis of synthetic calcium carbonate polymorphs using FT-IR spectroscopy.* Talanta, 2003. **59**(4): p. 831-836.
38. Reig, F.B., J.G. Adelantado, and M.M. Moreno, *FTIR quantitative analysis of calcium carbonate (calcite) and silica (quartz) mixtures using the constant ratio method. Application to geological samples.* Talanta, 2002. **58**(4): p. 811-821.
39. Chakrabarty, D. and S. Mahapatra, *Aragonite crystals with unconventional morphologies.* Journal of materials chemistry, 1999. **9**(11): p. 2953-2957.

40. Culka, A., J. Jehlička, and I. Němec, *Raman and infrared spectroscopic study of boussingaultite and nickelboussingaultite.* Spectrochimica Acta Part A: Molecular and Biomolecular Spectroscopy, 2009. **73**(3): p. 420-423.
41. Balan, E., et al., *First-principles study of the OH-stretching modes of gibbsite.* American Mineralogist, 2006. **91**(1): p. 115-119.
42. Popescu, C.-M., M.-C. Popescu, and C. Vasile, *Structural analysis of photodegraded lime wood by means of FT-IR and 2D IR correlation spectroscopy.* International journal of biological macromolecules, 2011. **48**(4): p. 667-675.
43. Synytsya, A., et al., *Fourier transform Raman and infrared spectroscopy of pectins.* Carbohydrate polymers, 2003. **54**(1): p. 97-106.
44. Saikia, B.J., G. Parthasarathy, and N. Sarmah, *Fourier transform infrared spectroscopic characterization of Dergaon H5 chondrite: Evidence of aliphatic organic compound.* Nature and Science, 2009. **7**(4): p. 45-51.
45. Ullah, S., et al., *Effect of expandable graphite and ammonium polyphosphate on the thermal degradation and weathering of intumescent fire-retardant coating.* Journal of Applied Polymer Science, 2021. **138**(17): p. 50310.
46. Cai, Y., J. Lv, and J. Feng, *Spectral characterization of four kinds of biodegradable plastics: poly (lactic acid), poly (butylenes adipate-co-terephthalate), poly (hydroxybutyrate-co-hydroxyvalerate) and poly (butylenes succinate) with FTIR and Raman spectroscopy.* Journal of Polymers and the Environment, 2013. **21**: p. 108-114.
47. Mishra, S., et al., *Vibrational spectroscopic signatures of hydrogen bond induced NH stretch–bend Fermi-resonance in amines: The methylamine clusters and other N–H⋯ N hydrogen-bonded complexes.* The Journal of Chemical Physics, 2020. **153**(19).
48. Işik, G., et al., *Determination of doxorubicin amount conjugated to mPEG-b-PCL copolymer via pH sensitive hydrazone bond.* Turkish Bulletin of Hygiene & Experimental Biology/Türk Hijyen ve Deneysel Biyoloji, 2022. **79**(2).
49. Pandiarajan, S., et al., *FT-IR and FT-Raman spectral studies of bis (L-proline) hydrogen nitrate and bis (L-proline) hydrogen perchlorate.* Journal of Raman Spectroscopy: An International Journal for Original Work in all Aspects of Raman Spectroscopy, Including Higher Order Processes, and also Brillouin and Rayleigh Scattering, 2005. **36**(10): p. 950-961.